

LQG/LTR Control of Small Flexible Spacecraft with Elastic Memory Composite Appendages

Joseph M. Fulton

Department of Astronautics, US Air Force Academy
2354 Fairchild Dr., USAF Academy, CO 80840; (719) 333-4110
joseph.fulton@usafa.af.mil

Scott Palo, Don Mackison

Department of Aerospace Engineering Sciences, University of Colorado
429 UCB, Boulder, CO 80309-0429; (303) 492-4289
scott.palo@colorado.edu, Mackison@colorado.edu

ABSTRACT: This paper looks at attitude control considerations for a small flexible spacecraft with a gravity gradient boom constructed from elastic memory composites. Free-free boundary conditions are used in the development of the system's equations of motion. Finite element model analysis generates the needed mode shape matrix and resonant frequencies. Modal coordinates are chosen over physical coordinates during the LQG/LTR controller design due to the greatly reduced number of states to control. Controller robustness and pole-zero cancellation techniques further reduce the order of the control transfer matrix. System performance characteristics are determined for the system in response to optimal maneuvering to nominal pointing following a momentum dumping procedure of the reaction wheels. The simulation identified the need to include the first resonant modes in the design model to ensure the system is robust in the presence of uncontrolled higher frequency modes and modeling errors.

INTRODUCTION

The trend in utilizing small satellites to accomplish space missions has been steadily increasing over the last two decades. Businesses, governmental organizations, and academic institutions find the reduced development costs and time lines, when compared to the larger conventional satellites, an appealing benefit when establishing a small satellite program. As the number of small satellite missions increase in the coming years, so too will the unique ways in which designers prepare for these missions. Working within mass, volume, and power constraints, satellite designers will "push the envelope" on what is possible to accomplish. These efforts will generate creative ways of solving complications experienced by former systems. Non-traditional methods of deploying structures on small satellites is one such emerging area of study.

Current research efforts conducted within the materials industry are looking into constructing deployable structures from elastic memory composites (EMC).¹ Strain energy is stored within appendages made from shape memory composites and can be released upon command by heating the material beyond its glass transition temperature. Shape memory mechanisms can eliminate the need for traditional highly complex

mechanical deployment devices, massive launch canisters, and independent deployment control systems.

A study conducted in 2002 by members of Composite Technologies Development, Inc (CTD) and ABLE Engineering looked at the impact of using EMC longerons in the CoilAble™ boom design for NASA's Space Solar Panel System.² While the longeron mass of a gravity gradient boom could be reduced up to a factor of ten while easily achieving effective strains of 2%, the impact such an appendage would have on the attitude control system of a small flexible spacecraft was not determined.

FLEXIBLE SPACECRAFT MODELING

The attitude motion of a flexible spacecraft is properly described by coupled sets of partial and ordinary differential equations. The rotational motion of the undeformed system, called the rigid body motion, is described by ordinary differential equations while the flexures are described by partial differential equations. The rigid body dynamics are derived from Euler's rotational equations of motion and include gravity gradient torques. Numerical finite element models are used to determine the mode shapes and natural frequencies as well as the mass, damping, and stiffness matrices of the flexible system.³ Assumed modes method is often used to couple the rigid body and flexible dynamics by using the spatial solutions of the

partial differential equations as assumed mode shapes and letting the modal coefficients serve as the generalized coordinates describing the flexures.

Free-Free Boundary Conditions

Historically, research in the area of flexible spacecraft control has focused on assuming cantilevered boundary conditions at the connection point between the spacecraft bus and the flexible appendage.⁴ The boundary conditions at one end have the appendage fixed in translation and rotation (see

Figure 1). This is a valid assumption when the total system center of mass is located close to the center of mass of the controlling body. Two examples of when this occurs is large space structures when $m_{CB} \gg m_{app}$ (where m_{CB} and m_{app} are the masses of the controlling body and the flexible appendage) and when flexible appendages are symmetrically orientated about the controlling body (as shown in Figure 2). The torque generated by the displaced appendage is applied at the connection point between the controlling body and the appendage. The torque experienced by the controlling body is in the same direction as it is generated from the appendage.

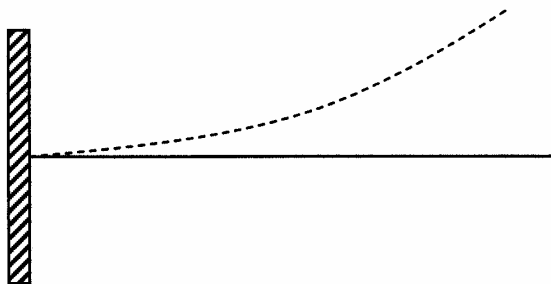


Figure 1. Illustration of Cantilever Appendage Conditions

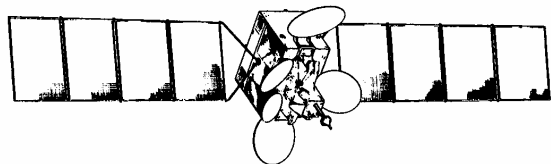


Figure 2. Three-Axis-Stabilized Geosynchronous Communications Satellite⁵

Assuming cantilever mode shapes simplifies several terms in the Lagrangian dynamics because the center of mass of the system experiences small variations. However, this assumption becomes less valid as the mass of the satellite bus is reduced and the appendage configuration does not take on a symmetric shape. As the system's center of mass moves further away from

the center of mass of the controlling body, larger displacements of the system's center of mass are realized in the body reference frame for the deformed spacecraft. This means the time rate of change of the system's inertia matrix is not zero and terms once neglected in the Lagrangian now need to be taken into consideration.

For a gravity gradient stabilized small satellite, the assumption of a cantilever appendage is no longer as valid as it is for a large space structure. This is especially true as the mass of the satellite gets closer to the mass of the attached appendage. A better approach is to consider the appendage as a free-free beam with attached lumped masses at either end for the satellite and tip mass (see Figure 3). Now, each end of the appendage is allowed to translate and rotate when determining the mode shapes used to couple the rigid body and flexible dynamics. This is a more realistic assumption when dealing with small satellites in that the attitude of the satellite is directly impacted by the motion of the appendage.

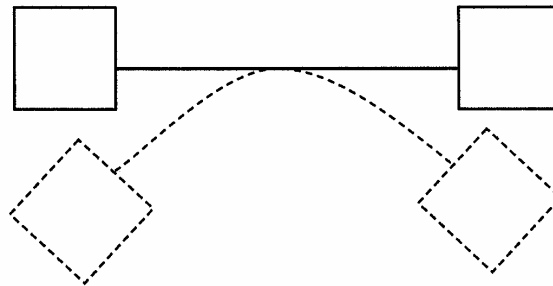


Figure 3. Illustration of Free-Free Appendage Conditions

Finite Element Model

The system model used for this paper is based off the structural properties of FalconSat-3, a small satellite designed at the US Air Force Academy.⁶ Reaction wheels located within the controlling body provide the required control torques while the attitude of the controlling body is determined from sun sensor and magnetometer information. The flexible appendage is a non-traditional gravity gradient boom constructed from Elastic Memory Composite (EMC) materials with a cubic tip mass. Table 1 lists the material properties for both beryllium copper,⁷ a common alloy used in traditional boom elements, and EMC materials.⁸ The composite material used in the finite element model (FEM) not only is more flexible but also has 15.7% the density of materials which traditional booms are constructed from.

Table 1. Material Properties of Beryllium Copper and EMC

	Beryllium Copper	EMC
Young's Modulus, E [GPa]	138	40.06
Poisson Ratio, ν	0.30	0.31
Shear Modulus, G [GPa]	53.1	15.29
Density, ρ [kg/m ³]	8830	1384

The EMC material properties were entered in MSC.Patran 2004 r2 to create a FEM of a free-free beam with lumped masses fixed at either end of the flexible appendage to represent the satellite and tip mass. Both the satellite and tip mass are free to translate and rotate. The lumped masses were treated as cubic shapes with uniform mass distribution. For a cubic shape with uniform mass distribution, the inertia about the object's center of mass is

$$I_{11} = I_{22} = I_{33} = \frac{ml^2}{6} \quad (1)$$

where m is the mass of the object, l is the length of a side and the products of inertia are equal to zero. Table 2 lists the properties entered into the FEM for the satellite and tip mass.

Table 2. Lumped Mass Properties Used in FEM Analysis

	Satellite	Tip Mass
Mass	40 kg	7 kg
Side Length	0.5 m	0.25 m
Inertia	1.667 kgm ²	0.0729 kgm ²

The beam representing the EMC flexible appendage is modeled as a hollow, cylindrical tube with properties shown in Table 3. 101 node points were used in the analysis evenly spaced 4 cm apart with the satellite's controlling body located at node 1 and the tip mass located at node 101. Each node is free to both translate and rotate. A normal modes solution type was selected to complete a full run of the entire model.

State Space Representation

The differential equations of motion for an undamped free vibration system are of the form⁹

$$[m]\ddot{x} + [k]x = F \quad (2)$$

where $[m]$ and $[k]$ are the mass and stiffness coefficients coupling each node, F is the matrix of external forces applied to the system, and x is the physical state vector containing the coordinates of each node. Since each node has 6 degrees of freedom, the dimensions of x is (606 x 1).

Table 3. Beam Properties Used in FEM Analysis

Property	Value
Total Length	4 m
Outer Diameter	2.54 cm
Thickness	0.46482 mm
Cross Sectional Area	73.5 mm ²
$I_{11} = I_{22}$	2.3×10^{-8} kgm ²

The state space representation of Eq. 2 requires a set of first order equations. This is done in the following manner:

$$\begin{aligned} \dot{x} + [m]^{-1}[k]x &= [m]^{-1}F \\ \dot{x} &= -[m]^{-1}[k]x + [m]^{-1}F \end{aligned} \quad (3)$$

Let

$$\begin{aligned} z_1 &= x \\ \dot{z}_1 &= \dot{x} \\ z_2 &= \dot{z}_1 \\ \dot{z}_2 &= -[m]^{-1}[k]z_1 + [m]^{-1}F \end{aligned} \quad (4)$$

Then

$$\begin{pmatrix} \dot{z}_1 \\ \dot{z}_2 \end{pmatrix} = \begin{pmatrix} 0 & I \\ -[m]^{-1}[k] & 0 \end{pmatrix} \begin{pmatrix} z_1 \\ z_2 \end{pmatrix} + \begin{pmatrix} 0 \\ [m]^{-1}F \end{pmatrix} \quad (5)$$

For this system model, F is the control torque moment acting on the controlling body located at node 1. Since there are three independent reaction wheels providing the control input, F takes the form

$$F = \begin{pmatrix} 0_{3 \times 3} \\ I_{3 \times 3} \\ 0_{600 \times 3} \end{pmatrix} u \quad (6)$$

Attitude measurements for this system are the rotational orientations of the controlling body and is represented as

$$y = Cz \quad (7)$$

where

$$C = \begin{bmatrix} 0_{3 \times 3} & I_{3 \times 3} & 0_{3 \times 600} & 0_{3 \times 606} \end{bmatrix} \quad (8)$$

since the measurements are the displacement rotations with no rate measurements.

Now, the state space representation of the system using physical coordinates, x , can become overwhelming depending on the number of nodes used in the FEM. For this case, the plant matrix, A , has dimensions (1212 x 1212). Computer processing capacity may be of little concern when using the latest desktop technology, but such luxury is typically not available to small satellites. A viable solution is found in the assumed modes method using a linear coordinate transformation known as the modal transformation.¹⁰

Let the displacement function of a deformed flexible system, shown in Figure 4, be expressed as

$$u(r, t) = \sum_{m=0}^{\infty} \phi_m(r) \eta_m(t) \quad (9)$$

where $\eta_m(t)$ is the m^{th} vibrational coordinate and $\phi_m(r)$ is the m^{th} normal mode shape of the mode shape matrix, $[\phi]$, whose columns are the eigenvectors of the system.

Since $[\phi]$ is spatial and η is temporal, we can insert Eq. 9 into Eq. 2 and get

$$[m][\phi]\ddot{\eta} + [k][\phi]\eta = F \quad (10)$$

Premultiplying by $[\phi]^T$ yields

$$[\bar{M}]\ddot{\eta} + [\bar{K}]\eta = \bar{F} \quad (11)$$

where the bar denotes a generalized matrix in modal equations and

$$\begin{aligned} [\bar{M}] &= [\phi]^T [m] [\phi] = [\bar{M}]^T \\ [\bar{K}] &= [\phi]^T [k] [\phi] = [\bar{K}]^T \\ \bar{F} &= [\phi]^T F \end{aligned} \quad (12)$$

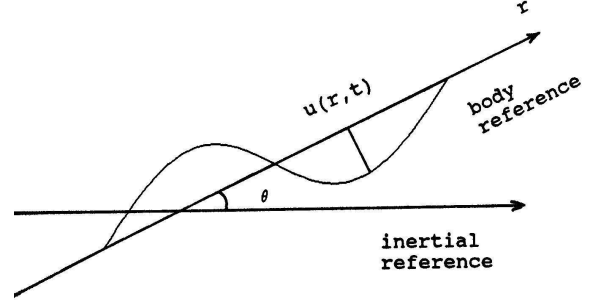


Figure 4. Displacement of the Flexible Appendage

If $[\phi]$ is orthonormal, then the generalized mass matrix, $[\bar{M}]$, is the identity matrix and the generalized stiffness matrix, $[\bar{K}]$, is a diagonal matrix whose elements are equal to the natural frequencies squared. Since both generalized matrices are diagonal, it makes the vibrational equations both inertially uncoupled and elastically uncoupled. This results in independent equations of flexible motion. If there are m mode shapes included in the analysis, these equations look like the following:

$$\begin{aligned} \ddot{\eta}_1 + \omega_{n1}^2 \eta_1 &= 0 \\ \ddot{\eta}_2 + \omega_{n2}^2 \eta_2 &= 0 \\ &\vdots \\ \ddot{\eta}_m + \omega_{nm}^2 \eta_m &= 0 \end{aligned} \quad (13)$$

where η_m is the m^{th} vibrational coordinate associated with the m^{th} mode shape and ω_{nm} is the m^{th} natural frequency. Therefore, η has dimensions of (1 x m).

The mode shape matrix, $[\phi]$ will have dimensions of (6n x m) where n is the number of nodes used in the finite element analysis and each node has six degrees of freedom (three translation and three rotation for each node). The number of nodal points used in the FEM analysis is up to the discretion of the researcher. However, a more accurate estimate of the deformation of the flexible system is found by using more points.

A damping ratio of 0.01 for the EMC material is assumed. This assumption is common for the structural

material industry when experimental data is not available.¹¹ Incorporating structural damping into the system model

$$\bar{D} = 2\zeta\sqrt{\bar{K}} \quad (14)$$

and applying the same development of Eq. 5 to Eq. 13, the state space representation of the modal equations becomes

$$\begin{pmatrix} \dot{\bar{z}}_1 \\ \dot{\bar{z}}_2 \end{pmatrix} = \begin{pmatrix} 0 & I \\ -\bar{K} & -\bar{D} \end{pmatrix} \begin{pmatrix} \bar{z}_1 \\ \bar{z}_2 \end{pmatrix} + \begin{pmatrix} 0 \\ \bar{F} \end{pmatrix} \quad (15)$$

and

$$\bar{y} = C[\phi]\bar{z} \quad (16)$$

Recall, the dimensions of the system plant, A , from Eq. 5 is (1212 x 1212). Now, the size of \bar{A} is dependent on the number of mode shapes included in the system model. There are an infinite number of mode shapes which can be generated for a flexible system. It is impossible to include all of the mode shapes since the accuracy which Patran can determine these mode shapes degrades at higher frequencies and the mode shape matrix, $[\phi]$, no longer is orthonormalized if the number of modes exceeds the number of nodes used in the FEM. A control designer can use the following technique to determine how many mode shapes to include in the nominal plant model.

The higher the frequency of a mode shape, the smaller the energy which is stored in that shape. Harmonic motion of the flexible structure will subject the controlling body to harmonic excitation. The

nondimensional ratio, $\frac{F_{tr}}{F_0}$, is a measure of the force transmitted to the controlling body and is written as⁹

$$\frac{F_{tr}}{F_0} = [1 + (\frac{2\zeta\omega}{\omega_n})^{1/2} |G(i\omega)|] \quad (17)$$

where ζ is the viscous damping factor, ω is the excitation frequency, ω_n is the natural frequency of undamped oscillation, and $|G(i\omega)|$ is the magnitude of the system's frequency response. For higher frequency resonant modes, the force transmitted to the controlling body decreases. In addition, the gain of a

stable system drops off at frequencies higher than the control dynamics of the closed loop system.

Using the system's free-free resonant frequencies produced from the FEM analysis, a plot is created of $\frac{1}{\omega_n^2}$ versus the resonant mode number. Resonant mode numbers represent each mode shape, with both bending modes in the x and y direction receiving one number instead of two separate numbers, see Figure 5.

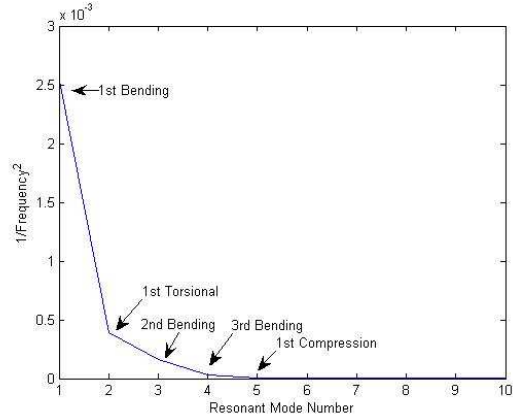


Figure5. Nondimensionalized Resonant Transmission Forces

Table 4. Free-Free Resonant Frequencies for Nominal Model

Mode Shape	Frequency (Hz)
Rigid Body Mode	8.3781 x 10 ⁻⁷
Rigid Body Mode	3.2062 x 10 ⁻⁶
Rigid Body Mode	3.9299 x 10 ⁻⁶
Rigid Body Mode	1.0974 x 10 ⁻⁵
Rigid Body Mode	1.2097 x 10 ⁻⁵
Rigid Body Mode	1.2959 x 10 ⁻⁵
1 st Bending in Y direction	3.1518
1 st Bending in X direction	3.1518
1 st Torsional Mode	8.0284
2 nd Bending in Y direction	12.588
2 nd Bending in X direction	12.588
3 rd Bending in Y direction	29.491
3 rd Bending in X direction	29.491
1 st Compression Mode	55.555
4 th Bending in Y direction	61.690
4 th Bending in X direction	61.690

Resonant modes beyond the fourth bending mode will be excluded from the nominal model because the slope of the plot approaches zero beyond that point. Table 4 lists the flexible modes, along with the rigid body modes generated in the FEM analysis, which are used

to build the nominal system model. These modes lead to a modal \bar{A} matrix of dimensions (32 x 32), which is 2.6% the size of the plant matrix generated using physical coordinates.

CONTROLLER DESIGN

A key design consideration is the controller effort generated by the reaction wheels. Since the flexible system is a gravity gradient appendage for a small satellite, it will take more control effort to correct pitch and roll displacements than yaw displacements. In this case, as well as for most flexible appendages, greater control effort is required to produce the same dynamic response one would experience from a three-axis stabilized cube. The small satellite limitations of mass, volume, and available power impact the torque produced from on board reaction wheels. The typical maximum torque produced by reaction wheels on small satellites is in the 0.02Nm to 0.3Nm range.^{12 13 14} It is possible, in the not too distant future, for more power to be made available to control actuators through improved power designs or increases in solar array efficiency. For this study, the maximum allowable control effort for the analysis of the system will be 3Nm.

Additionally, the assumed mission of this small flexible spacecraft will be to meet the attitude requirements of the FalconSat-3 scientific payloads. The attitude control system needs to keep these payloads pointed $\pm 5^\circ$ in the ram, or velocity, direction. This requirement applies to both yaw and pitch while no hard requirement is placed on the roll of the controlling body. A performance metric provided by the scientists states that while data is usable within 5° off nominal, the accuracy of the data degrades the further away from 0° the payloads are pointed.

An optimal controller is designed using Linear Quadratic Gaussian regulators with Loop Transfer Recovery (LQG/LTR) techniques¹⁵ to minimize the time it takes to reach nominal pointing requirements once pitch/yaw are off 5° nominal while operating within the control effort limit of 3Nm. This initial displacement is a result of the reaction wheels periodically reaching saturation and momentum dumping is used in conjunction with despinning the wheels. The scientists are concerned with how much time is required for the payloads to go from 5° to 0° and reach a steady state such that vibrations induced by the flexible appendage have minimal impact on system dynamic response.

LQG/LTR

Since the system is represented as

$$\begin{aligned}\dot{x} &= Ax + Bu \\ y &= Cx\end{aligned}\quad (18)$$

a cost function can be defined as

$$J = \frac{1}{2} \int_0^T (x'Qx + u'Ru)dt \quad (19)$$

where J is minimized with respect to the control input u(t).

J represents the weighted sum of energy of the state and control. Q and R are weighting matrices, or design parameters, where the state-cost matrix, Q, weights the states while the performance index matrix, R, weights the control effort. If Q is increased while R remains constant, the settling time will be reduced as the states approach zero at a faster rate. This means that more importance is being placed on keeping the states small at the expense of increased control effort. If R is very large relative to Q, the control energy is penalized very heavily. This physically translates to smaller motors, actuators, and amplified gains needed to implement the control law.

The LQR solution is basically a state feedback type of control, meaning it requires that all states be available for feedback. This is usually unreasonable and some form of state estimation is necessary. The LQG combines the design methods of LQR with optimal estimation, the Kalman filter. If unbiased white Gaussian noise is added to Eq. 18 such that

$$\begin{aligned}\dot{x} &= Ax + Bu + \omega \\ y &= Cx + \nu\end{aligned}\quad (20)$$

where ω represents random noise disturbance input (process noise) and ν represents random measurement (sensor) noise.

Combining the LQR controller

$$\begin{aligned}u &= -K\hat{x} \\ K &= R^{-1}B'P \\ 0 &= A'P + PA + Q - PBR^{-1}B'P\end{aligned}\quad (21)$$

with the optimal estimator

$$\begin{aligned}\dot{\hat{x}} &= A\hat{x} + Bu + L(y - C\hat{x}) \\ L &= \Sigma C' R_0^{-1} \\ 0 &= A\Sigma + \Sigma A' + Q_0 - \Sigma C' R_0^{-1} C\Sigma\end{aligned}\quad (22)$$

the LQR results in an asymptotically stable closed loop system.

The major problem with the LQG solution is its lack of robustness. The loop transfer recovery (LQG/LTR) technique maintains the LQG machinery but modifies the design procedure to address some of the shortcomings of the original LQG approach.

The open loop transfer function of the LQR is given by

$$L(s) = K\Phi(s)B \quad (23)$$

where $\Phi(s) = (sI - A)^{-1}$.

The open loop transfer function for LQG is likewise given by

$$L(s)_{LQG} = K(sI - A + BK + LC)^{-1} LC\Phi(s)B \quad (24)$$

Under the following two conditions

1. $G(s)$ is minimum-phase (i.e. it has no zeros in the RHP)
2. $R_0 = 1$ and $Q_0 = q^2 BB'$

it can be shown that¹⁶

$$\lim_{q \rightarrow \infty} L(s)_{LQG} = L(s) \quad (25)$$

This suggests the following procedure for design. Choose the LQR parameters (Q and R) such that the LQR loop transfer function, $L(s)$, also called the target feedback loop (TFL), has desirable time and/or frequency domain properties. Design an observer with parameters specified in (2) above. Increase the tuning parameter, q , until the resulting loop transfer function is as close as possible to the TFL. Because the loop transfer function of LQG approaches that of LQR, it will asymptotically recover its properties.

To accomplish the recovery step, select a scalar, q , and solve the filter Riccati equation

$$A\Sigma + \Sigma A' + q^2 BB' - \Sigma C' C\Sigma = 0 \quad (26)$$

and set $L = \Sigma C'$.

The higher the value of q , the closer the LQG system comes to the LQR performance. It should be noted that the value of q should not be increased indefinitely because this may lead to unreasonably large values for the filter gain. Also, because LQR has -20dB slope at high frequencies, large values of q will also recover this slow roll-off rate. Smaller values for q will tend to trade off lower stability margins with higher roll-off rates at higher frequencies.

Controller Robustness

Uncontrolled modes, as well as the error in the knowledge of the controlled modes, represent uncertainty. Since the number of structural modes is usually large and finite element modeling accuracy typically decreases with increasing modal frequency, the design model should consist of the rigid body modes plus the first few elastic modes. The remaining structural modes then constitute the plant uncertainty. The uncertainty barrier is a measure of the plant uncertainty at high frequencies. The plant uncertainty can be represented as either multiplicative or additive uncertainty (see Figure 6).

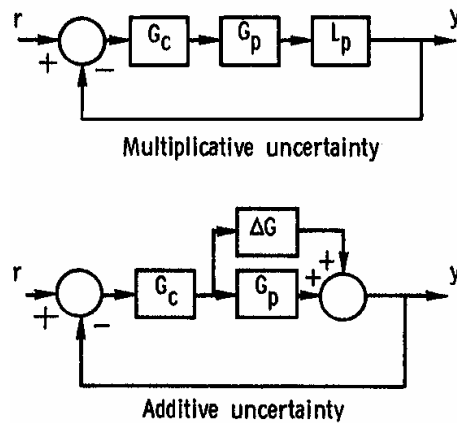


Figure 6. Defining Uncertainty in a Model

The multiplicative uncertainty form is preferred in the literature on robustness because the compensated transfer function has the same uncertainty representation as the nominal model. However, since flexible structure models exhibit naturally the additive uncertainty form of the transfer function matrix, this will be used.

With the additive uncertainty formulation, a sufficient condition for stability robustness is given by

$$\frac{\underline{\sigma}(I + G_p G_c)}{\overline{\sigma}(G_c)} > \overline{\sigma}(\Delta G) \quad (27)$$

where G_p and G_c are the design model plant and compensator transfer matrices, and $\overline{\sigma}$ and $\underline{\sigma}$ denote the largest and smallest singular values. At high frequencies, assuming $\|G_p G_c\| \ll 1$, Eq. 27 approximately yields

$$\overline{\sigma}(G_c) < \frac{1}{\overline{\sigma}(\Delta G)} \quad (28)$$

that is, the compensator must roll off sufficiently rapidly at high frequencies to remain robust in the face of unmodelled/uncertain high frequency structural modes and noise. The main objective of the LQG/LTR approach is to first design a full state compensator which has the behavior of the desired loop transfer matrix (i.e. the loop gain $G_p G_c$). Therefore, any loop shaping should involve the product $G_p G_c$ rather than G_c alone as in Eq. 27 and Eq. 28. Assuming G_p is a square matrix

$$\begin{aligned} G_c &= G_p^{-1}(G_p G_c) \\ \overline{\sigma}(G_c) &\leq \overline{\sigma}(G_p^{-1})\overline{\sigma}(G_p G_c) \\ \overline{\sigma}(G_c) &\leq \underline{\sigma}^{-1}(G_p)\overline{\sigma}(G_p G_c) \end{aligned} \quad (29)$$

Substituting Eq. 29 into Eq. 27, the following sufficient condition for stability robustness is obtained:

$$\frac{\underline{\sigma}(I + G_p G_c)\underline{\sigma}(G_p)}{\overline{\sigma}(G_p G_c)} > \overline{\sigma}(\Delta G) \quad (30)$$

Pole-Zero Cancellation

Looking at the robustness of the controller in the presence of unmodeled higher frequency modes most often leads to lower order controllers than those that are required to control the nominal plant. This is a result of the design model being lower in order due to the inclusion of the lower frequency modes while high frequency modes are lumped into the uncertainty of the system dynamics. It may be possible to further reduce the order of the controller when pole-zero cancellation is taken into consideration.

Consider a design model where the six rigid body modes are included as well as the first resonant modes about each axis. This will generate a controller of order 18, meaning there are 18 poles in the controller transfer function. Since the small flexible spacecraft is a multi-input multi-output (MIMO) system using three controller inputs and measuring three angular displacements, the controller is comprised of nine transfer functions all of the order 18. This high order of the controller may be unnecessary if some of the controller poles are in close proximity to controller zeros.

There is no magic number to identify if the controller poles and zeros are within close proximity of each other or not. Instead, a useful technique in further reducing the order of the controller is to evaluate the effect on dynamic response if some poles are allowed to cancel out with zeros in close proximity. The Matlab command `minreal`, minimal realization, is a useful tool in accomplishing pole-zero cancellation. It is a straightforward search through the poles and zeros looking for matches that are within tolerance.¹⁷ The default tolerance is $\sqrt{\textit{eps}}$, where *eps* is machine precision. The tolerance value can be increased to force additional cancellations as long as the Bode plots match up with the unreduced controller. If there is a slight difference in the Bode plots, a comparison between the dynamic response of the reduced controller and the controller prior to pole-zero cancellation will indicate whether the tolerance was set to too high of a value. If the dynamic response shows little change, this may indicate that while a certain pole-zero cancellation may generate differing Bode plots, the contribution of that particular pole-zero pair is not significant enough to alter the system response drastically.

SIMULATION RESULTS

A Matlab file was created to read in the FEM data and generate the mode shape matrix for both the nominal and design model as well as the natural frequencies for each mode. Simulations were run using Simulink to plot the system response to the LQG/LTR controller (see Figure 7). Since the roll and pitch axes will require more control effort, an initial angular displacement of 5° is applied to the pitch axis and the controller is trying to bring the system to a desired attitude of roll = 0°, pitch = 0°, and yaw = 0°. The simulation generates both the control effort and dynamic response for both the flexible system.

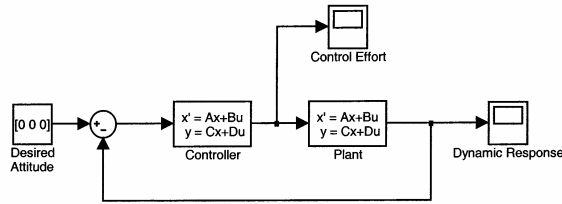


Figure 7. Simulink Block Diagram for Closed Loop Response

Iterative modifications of the LQG/LTR design parameters were required to bring the reaction wheel control efforts within the 3Nm limit. Final values used for the design parameters Q and R for the LQR calculation, Q_0 and R_0 for the Kalman filter, and q for the LTR calculation are listed in Table 5 and the subsequent control effort required is shown in Figure 8.

Table 5. Final Values for Design Parameters

Design Parameter	Value
Q	$0.01 * I_{n \times n}$
R	$I_{3 \times 3}$
Q_0	variance of 1
R_0	variance of 0.01
q	[1 1e2 1e4 1e6]
Max Control Effort	3Nm

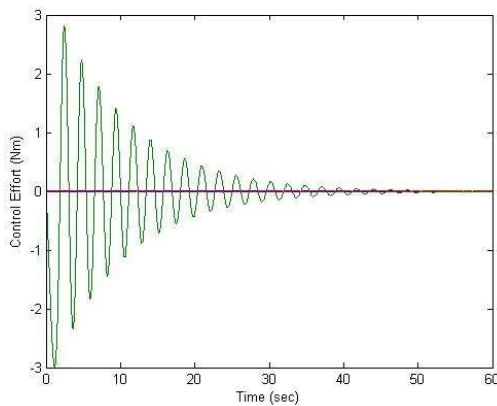


Figure 8. Control Effort with Final Design Parameters

The stability robustness test is evaluated to determine which resonant modes, if any, need to be included in the design model. The stability robustness (SR) barrier is crossed if only rigid body modes are retained in the design model while all of the resonant modes are placed in the uncertainty transfer matrix (see Figure 9). This violation of the SR barrier occurs at the same frequency as the first bending mode.

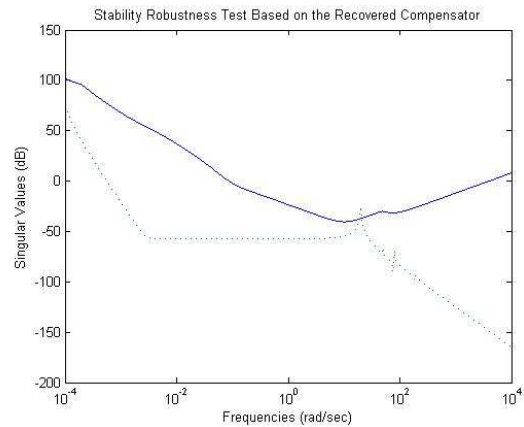


Figure 9. Baseline SR Test for Rigid Body Modes Only

To ensure the flexible system meets SR requirements, resonant modes need to be included in the design model. Figure 10 is a plot of the SR barrier when the first resonant modes about each axis are included. This design model has a SR value of 41 dB in the frequency region of the second bending mode. The upper curve sloping upwards indicates good tolerance of high-frequency uncertainty.

The SR value can be improved if more resonant modes are included in the design model. Performance of the closed loop system depends on the low-frequency gain and crossover frequency of the loop transfer matrix $G_p G_c$. Larger values indicate better tracking performance. Any increase in gain to improve tracking performance will decrease the stability robustness. Since the system model already takes into consideration the maximum control effort produced by the reaction wheels, an increase in bode gain will exceed this limit.

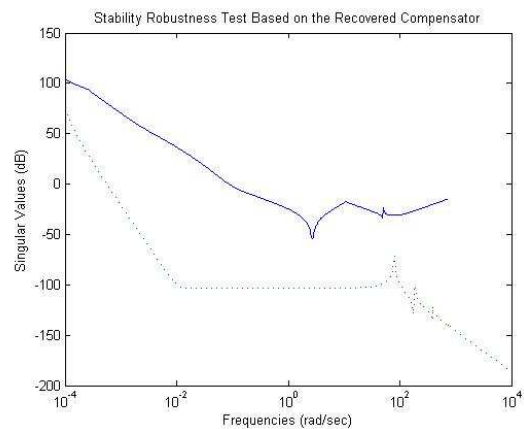


Figure 10. Baseline SR Test with First Resonant Modes

In addition, the cost of needlessly adding higher frequency resonant modes may prove detrimental to onboard processor limitations. The LQG/LTR process generates a controller of the same order as the system plant. The controller for a design model containing the first resonant modes is a 3 by 3 matrix of transfer functions, each the ratio of a 17th order polynomial to a 18th order polynomial. It would require programming 333 coefficients to implement this controller. By adding the second bending modes to the design model, the order of the controller is increased to 22 and requires an additional 72 coefficients. The inclusion of the first bending mode in both the x and y directions and the first torsional mode is enough to satisfy the stability robustness of the controller and the inclusion of higher resonant modes is not required.

To illustrate the pole-zero cancellation technique, consider the pole-zero map of the controller transfer function going from input 1 to output 1, $G_c(1,1)$, shown in Figure 11. It is apparent several controller poles lie in close proximity to controller zeros. Cancellations may occur as long as the Bode plots of the reduced controllers, as well as the system dynamic response, match those of the unreduced controllers.

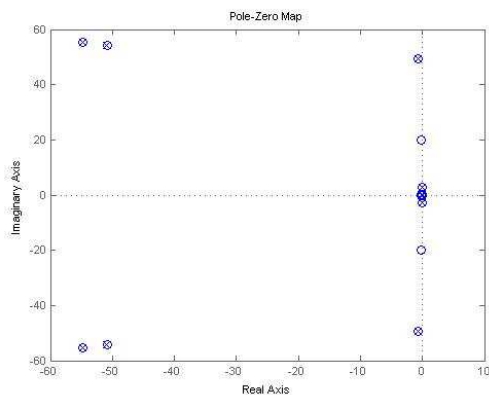


Figure 11. Pole-Zero Map of $G_c(1,1)$

Recall that the default tolerance value for the Matlab mineral command is $\sqrt{\text{eps}}$. It is possible to reduce this tolerance, making the value larger, and generate the same Bode plot of the reduced controller as the unreduced one. As long as the plots for both the full and reduced order controllers match up, then the dynamics of both controllers are similar. For example, consider the controllers if the default tolerance setting is used, $\sqrt{\text{eps}}$, for the transfer function going from input 1 to output 1, $G_c(1,1)$. From Figure 12, one can see how the reduced order controller (x's) matches up with the

full order controller (solid line) in both magnitude and phase, for both low and high frequencies.

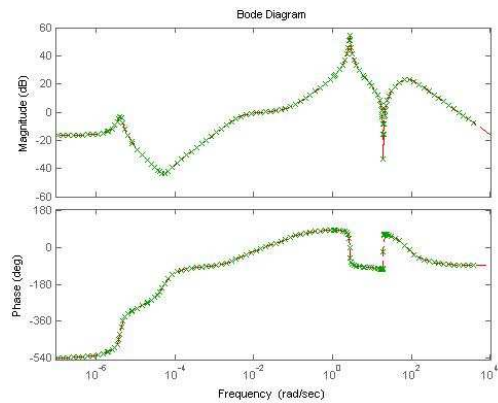


Figure 12. Comparison of Reduced and Full Order Controllers (default tol)

One may relax the tolerance in the minimum realization until a divergence in the Bode plots is noticed. A better approach is to run a sweep of tolerance values and, instead of visually comparing the Bode plots, calculate the RMS values and plot those values vs. the tolerance step. The tolerance is stepped from $\sqrt{\text{eps}}$ to 1e-1 in orders of magnitude such that tolerance step 1 is $\sqrt{\text{eps}}$, tolerance step 2 is 1e-7, tolerance step 3 is 1e-6, and so on out to tolerance step 8 equaling 1e-1. The RMS of the Bode plots are calculated for both magnitude and phase for all 9 controller transfer functions. Since the previous plot was for $G_c(1,1)$, the following two plots are the RMS plots for the same transfer function.

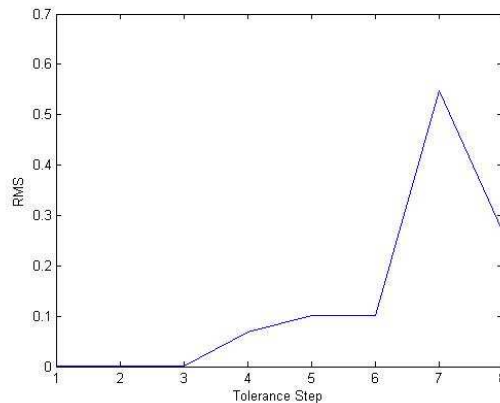


Figure 13. RMS of Bode Magnitude for $G_c(1,1)$

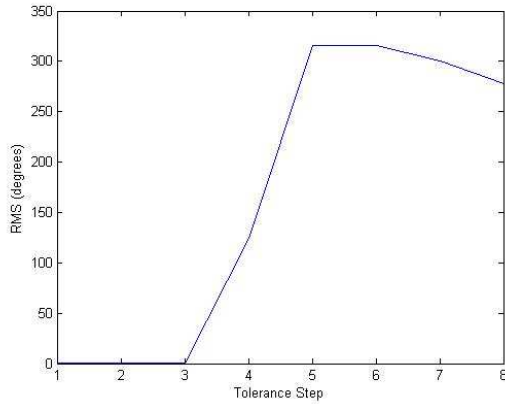


Figure 14. RMS of Bode Phase for $G_c(1,1)$

Looking at Figure 13 and Figure 14, a noticeable change in RMS values occurs between tolerance steps 3 and 4 ($1e-6$ and $1e-5$). This means a noticeable change in the reduced order controller dynamics occurs when additional pole-zero cancellations are performed beyond a tolerance of $1e-6$. Figure 15 and Figure 16 show the Bode comparisons for both tolerance steps.

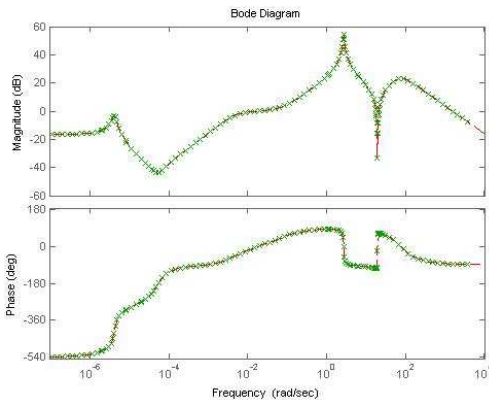


Figure 15. Comparison of Reduced and Full Order Controllers (tol = $1e-6$)

Notice how the two Bode plots differ once the RMS is noticeable. This would lead one to believe that the tolerance limit should be set at $1e-6$. However, note how the plot in Figure 16 diverges at low frequencies. This is in the rigid body region of the system; a location where the poles and zeros are in close proximity to each other and the origin of the s -plane. It is expected to see more cancellations occurring in this region than in the regions where the distance from the s -plane origin (i.e. frequency) is greater.

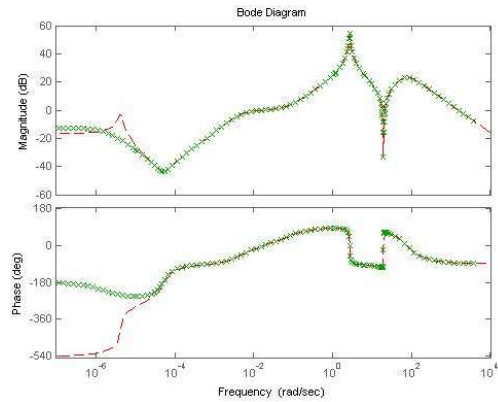


Figure 16. Comparison of Reduced and Full Order Controllers (tol = $1e-5$)

Looking at the simulation results of how the system responds to the reduced order controller shows no noticeable difference between tolerance step 3 or 4. Instead of visually determining this, RMS values can be calculated and plotted in the same manner as above for both control effort and dynamic response of the system. The following two figures plot these RMS values.

From Figure 17 and Figure 18, a noticeable change in RMS values occurs between tolerance steps 6 and 7 ($1e-3$ and $1e-2$). A design consideration is to limit the pole-zero cancellation by using either the controller dynamics or the overall system dynamics. With the controller approach, the reduced controller closely resembles the dynamics of the full order controller. However, the cost of this approach is an increased number of coefficients required to code up the controller. If the system dynamics approach is used, a smaller number of coefficients will be needed.

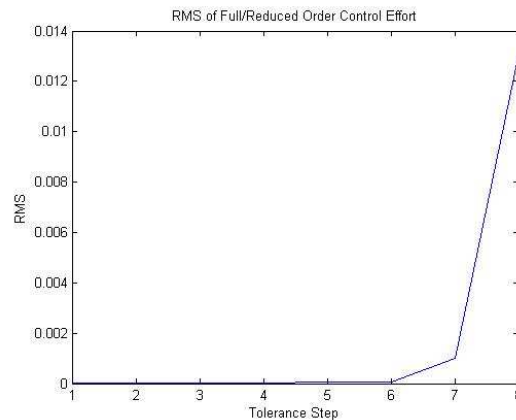


Figure 17. RMS of Full/Reduced Order Control Effort

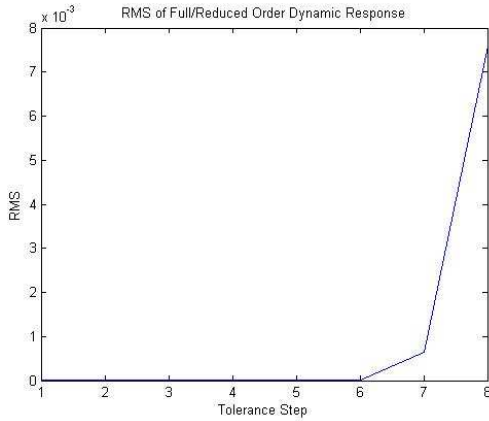


Figure 18. RMS of Full/Reduced Order Dynamic Response

To illustrate this, the design model is comprised of the rigid body modes along with the first vibrational mode about each axis. For the full order system, 333 coefficients are required. For the Bode dynamics approach to pole-zero cancellation, 245 coefficients are required. The system dynamic approach only needs 108 coefficients (32.4% of the full order requirement).

The SR plot using the reduced controller is shown in Figure 19 and generates the same stability robustness as that shown in Figure 10 for the full order controller. Figure 20 and Figure 21 compare the full order controller performance to the reduced order controllers. From the singular value plots, the control effort, and dynamic response, it is apparent that the reduced order controller has the same dynamic response as the full order LQG/LTR controller.

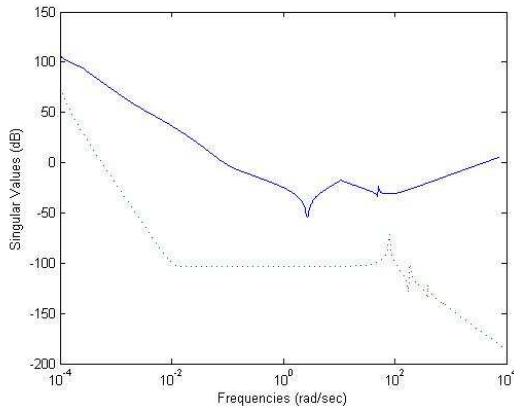


Figure 19. Stability Robustness Test Using Reduced Controller

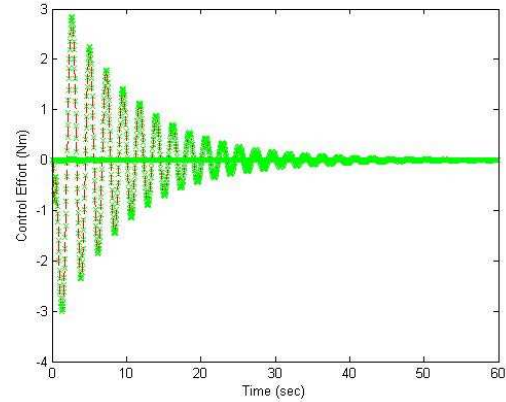


Figure 20. Control Effort of Full and Reduced Order Controllers

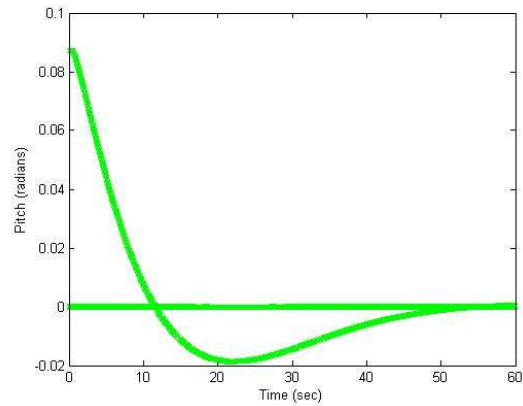


Figure 21. Dynamic Response of Full and Reduced Order Controllers

Transient system performance is often described in terms of the unit step function response. Since the input into the system is optimally shaped, the system performance specifications are similar with the following definitions. Dynamic delay time is the time required for the system to reach 50% the initial displacement value. Dynamic rise time is the time required for the response to go from 90% to 10% of its initial value. The time which the system response settles within 2% of its initial value is the dynamic settling time. Dynamic peak overshoot is the maximum difference between the transient and steady state solution and is represented as a percentage of the initial displacement.

Another performance specification which is measured is the crossover frequency, ω_0 , of the loop transfer matrix. While the stability margin is an indicator of the system performance, the crossover frequency determines the speed of the system response. A higher

value for ω_0 means faster response. The crossover frequency is determined by the frequency at which the minimum singular value of the loop transfer matrix, $G_c G_p$, has a gain of 0 dB (see Figure 22). System performance specifications for the modeled small flexible spacecraft using an EMC gravity gradient boom are listed in Table 6.

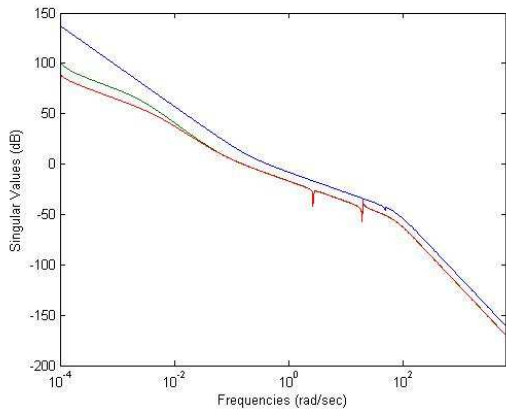


Figure 22. Singular Values of Recovered Loop Transfer Matrix, $G_c G_p$

Table 6. System Performance

Dynamic Performance	Value
Delay Time	4.1 sec
Rise Time	8.2 sec
Settling Time	48.8 sec
Peak Overshoot	21.3%
Stability Robustness	41 dB
Crossover Frequency	0.025 Hz

CONCLUSIONS

Order reduction techniques applied to the LQG/LTR optimal controller resulted in approximately one third of the necessary coefficients needed to implement the design when compared to a full order controller. This result will aid satellite designers in allocating on-board processor resources. The small flexible spacecraft is able to achieve a nominal pointing direction, following a momentum dumping maneuver of the reaction wheels, in less than a minute. This finding exceeded the expectations of the payload scientists who feared poor data collection durations averaging 15 minutes. The primary cause of the concern rested in the utilization of a non-traditional gravity gradient boom constructed from elastic memory composites, a system which does not have any flight heritage. A successful integration of the boom into the next FalconSat spacecraft may provide an opportunity to generate flight heritage with

the system before the end of 2010. This will offer a new way of deploying flexible space structures without the disadvantages of traditional systems.

REFERENCES

1. Tupper, M. L. et al., "Developments in Elastic Memory Composite Materials for Deployable Spacecraft Structures." 2001 IEEE Aerospace Conference. March 10-17, 2001. IEEE paper no. 3673.
2. Lake, Mark S. et al. "Application of Elastic Memory Composite Materials to Deployable Space Structures." AIAA Space 2001 Conference and Exposition. August 28-30, 2002. AIAA paper no. 2001-4602.
3. Bryson, Arthur E., Jr. "Notes on Guidance and Control." American Astronautical Society, Rocky Mountain Guidance and Control Conference. February 1983.
4. Nurre, D. S., Ryan, R. S., Scofield, H. N., and J. L. Sims. "Dynamics and Control of Large Space Structures," Journal of Guidance, Control, and Dynamics, vol. 7, No. 5, 514-526, 1984.
5. Wie, Bong. Space Vehicle Dynamics and Control, American Institute of Aeronautics and Astronautics, Inc: Washington, DC, 1998.
6. Space Systems Research Center, United States Air Force Academy, CO. "FalconSat-3 Critical Design Review", in house document, February 2004.
7. "ASM Materials Handbook," Materials Park, OH. 1990.
8. Space Systems Research Center, United States Air Force Academy, CO. "FalconSat-3 Boom System Critical Design Review," in house document. 15 June 2004.
9. Meirovitch, L. Elements of Vibration Analysis, 2nd edition. McGraw-Hill, Inc: Boston, MA, 1986.
10. Mackison, D. L. Guaranteed Cost Control of Flexible Space Structures. Ph.D. Dissertation, University of Colorado, Boulder, CO, 1988.
11. Chandra, Singh, and Gupta. "Damping Studies in Fiber-Reinforced Composites -- A Review," Composite Structures, vol. 46, 41-51, 1999.

12. Krogstad, T. R. Attitude Control of Satellites in Clusters. Master's Thesis, NTNU, Trondheim, June 2005.
13. Morrissey, J. R., Quinn, T. H., and G. Parcelli. "Attitude Determination and Control Subsystem for Spartan Life Spacecraft." Proceedings of the 11th Annual AIAA/USU Conference on Small Satellites, September 1997.
14. Zimbelman, D., Wilmont, J., and S. Evangelista. "The Attitude Control System Design for the Transition Region and Control Explorer Mission." Proceedings of the 10th Annual AIAA/USU Conference on Small Satellites, September 1996.
15. Blaloch, P. A. and D. L. Mingori. "Modified LTR Robust Control for Flexible Structures." Proceedings of the AIAA Guidance, Navigation and Control Conference. 314-318. 1986.
16. Stefani, R. T., Savant, C. J., Shahian, B., and G. H. Hostetter. Design of Feedback Control Systems (3rd edition). Saunders College Publishing: Boston, 1994.
17. MathWorks. Control System Toolbox User's Guide (5th edition). 2005.